J. Plasma Physics (2002), *vol.* 68, *part* 5, *pp.* 363–388.
DOI: 10.1017/S0022377802002040 Printed in the United Kingdom

Spectral and evolutionary analysis of advection–diffusion equations and the shear flow paradigm

A. THYAGARAJA,[1] N. LOUREIRO[2] and P. J. KNIGHT[1]

[1]EURATOM/UKAEA Fusion Association, Culham Science Centre, Abingdon OX14 3DB, UK

[2]Plasma Physics Group, Imperial College of Science, Technology and Medicine, London SW7 2BZ, UK
(a.thyagaraja@ukaea.org.uk)

(Received 7 September 2002)

Abstract. Advection–diffusion equations occur in a wide variety of fields in many contexts of active and passive transport in fluids and plasmas. The effects of sheared advective flows in the presence of irreversible processes such as diffusion and viscosity are of considerable current interest in tokamak and astrophysical contexts, where they are thought to play a key role in both transport and the dynamical structures characteristic of electromagnetic plasma turbulence. In this paper we investigate the spectral and evolutionary properties of relatively simple, linear, advection–diffusion equations. We apply analytical approaches based on standard Green function methods to obtain insight into the nature of the spectra when the advective and diffusive effects occur separately and in combination. In particular, the physically interesting limit of small (but finite) diffusion is studied in detail. The analytical work is extended and supplemented by numerical techniques involving a direct solution of the eigenvalue problem as well as evolutionary studies of the initial-value problem using a parallel code, CADENCE. The three approaches are complementary and entirely consistent with each other when an appropriate comparison is made. They reveal different aspects of the properties of the advection–diffusion equation, such as the ability of sheared flows to generate a direct cascade to high wave numbers transverse to the advection and the consequent enhancement of even small amounts of diffusivity. The invariance properties of the spectra in the low diffusivity limit and the ability of highly sheared, jet-like flows to 'confine' transport to low shear regions are demonstrated. The implications of these properties in a wider context are discussed and set in perspective.

1. Introduction

The simplest of all transport equations is the advection–diffusion equation characterizing 'passive scalar' transport by a specified velocity field. This type of equation has been analysed over many years by many authors. It continues to form a key core of fluid and plasma transport theory. Perhaps, somewhat surprisingly, there remain important features of such equations which have yet to be fully elucidated. The most recent manifestation of advection–diffusion phenomena are

those encountered in fusion plasmas where the so-called 'zonal' $\mathbf{E}\times\mathbf{B}$ flows (see [1–6]) have been identified as important elements in the formation of internal and edge transport barriers. Transport barriers are regions of high gradients of density and/or temperature that form spontaneously and which appear to be closely associated with zonal flows. These are $\mathbf{E}\times\mathbf{B}$ flows transverse to the magnetic field associated with a 'radial' electric field normal to the equilibrium flux surfaces. Such flows are thought, on the one hand, to be driven by the turbulence itself via the so-called 'Reynolds stresses' (in addition to purely neoclassical drives), and on the other hand, to exert a stabilizing influence on the turbulence.

The purpose of the present paper is to understand and lay bare the essential features of the interaction between flows and transport of some property, such as temperature or density (or the *turbulent fluctuations* in such quantities). The phenomenon is simplified to its essentials by taking the flow to be *given*, and assigning specific properties such as shear so that the model used captures the key features of more complicated systems. The diffusivity is also assumed to be known. The equation for passive transport is then linear, but turns out to be far from trivial, as one still has to deal with a non-self-adjoint, dissipative system. It will be shown that even this simplified model possesses a number of unexpected and remarkable spectral properties which throw light on the evolution of advection–diffusion problems in more complicated (including non-linear) physical situations [5]. In this connection, references [7, 8] may also be consulted for additional examples of the utility of the spectral approach in understanding the properties of equations encountered in plasma and fluid theory. Furthermore, the advection–diffusion equation is used as the simplest, paradigmatic example to model a specific domain decomposition approach to parallel computations of turbulence.

The paper is organized as follows. In Sec. 2 we discuss the mathematical formulation of the linear advection–diffusion model and analytical properties of the system. In Sec. 3, the numerical and analytical solutions to certain solvable cases of the system are presented and their properties discussed. Sec. 4 is devoted to the solution of the initial-value problem and the evolutionary approach using the parallel processing code CADENCE, which presents a typical example of the approaches taken in the computational physics of fully non-linear plasma turbulence simulations. The paper concludes with some discussion of the results and the contexts in which the insights obtained lead to useful conclusions.

2. Formulation of the model and analytic results

We consider a simple two-dimensional problem. Let R be a two-dimensional domain defined by the rectangle, $0 \le x \le L_x, 0 \le y \le L_y$. We shall be interested in a scalar function, $f(x, y, t)$ which is assumed to be periodic in y/L_y, with period 2π, and which satisfies (for simplicity) homogeneous boundary conditions at $x = 0, L_x$. We also suppose that ν is a uniform and constant diffusivity. It is useful to make contact with tokamak physics and refer to the x-direction as 'radial' and the y-direction as 'poloidal'. It is noted, however, that these are merely labels introduced to aid intuition. The basic model we start with is represented by the advection–diffusion equation,

$$\frac{\partial f}{\partial t} + v_y(x)\frac{\partial f}{\partial y} = \nu\left(\frac{\partial^2 f}{\partial x^2} + \frac{\partial^2 f}{\partial y^2}\right), \tag{1}$$

where the advecting velocity, $v_y(x)$ is assumed to be a *given* function of x. The equation states that under the influence of $v_y(x)$, the function f (this may represent temperature, magnetic flux, density or any other physical quantity of interest) is *advected* in the poloidal direction, but *diffused* in the radial and poloidal directions. Our fundamental problem therefore consists of elucidating the interplay of the advection and diffusion in this simple system.

We begin the analysis by noting some elementary facts pertaining to our model. (a) Equation (1) is linear, and the initial-boundary problem thus posed is easily shown to have a unique solution for 'reasonable' initial data on f and suitable v_y. (b) The system is always stable, irrespective of v_y. This follows from the 'H-theorem', which is readily obtained by integrations by parts:

$$\frac{d}{dt}\left(\int_0^{L_x}\int_0^{L_y} f^2\,dx\,dy\right) = -\nu\int_0^{L_x}\int_0^{L_y}\left[\left(\frac{\partial f}{\partial x}\right)^2 + \left(\frac{\partial f}{\partial y}\right)^2\right]dx\,dy. \tag{2}$$

(c) If the diffusivity $\nu = 0$, the equation can be solved exactly and the solution reveals that although there are an infinite number of conserved constants, and the equation is fully time-reversible, one obtains a very strong 'direct cascade' of energy in k_x, the radial wave number. In other words, the function $f(x, y, t)$ evolving according to the diffusionless equation quickly develops, on a time-scale to be determined shortly, extreme fine structure in the *radial* direction. (d) For many purposes, it is not necessary to consider diffusion in the y-direction. All the effects considered occur even when only diffusion in the x-direction, transverse to the advection, is retained.

We now demonstrate the direct cascade property alluded to above. Since f is periodic in y, we develop the solution in a Fourier series:

$$f(x, y, t) = \sum_{-\infty}^{\infty} \hat{f}_m(x, t)\,\exp(i2\pi my/L_y). \tag{3}$$

Substituting in (1), we find that the amplitudes satisfy the infinite set of equations,

$$\frac{\partial \hat{f}_m}{\partial t} = -ik_y v_y(x)\hat{f}_m - \nu k_y^2 \hat{f}_m + \nu\frac{\partial^2 \hat{f}_m}{\partial x^2}, \tag{4}$$

where $k_y \equiv 2\pi m/L_y$, and $m = 0, \pm1, \pm2, \ldots$. Now suppose that $\nu \equiv 0$. The explicit solution for the equation is then given by

$$\begin{aligned} f(x, y, t) &= \sum_{-\infty}^{\infty} \hat{f}_m(x, 0)\,\exp[ik_y(y - v_y t)] \\ &= F_0(x, y - v_y(x)t), \end{aligned} \tag{5}$$

where $f(x, y, 0) = F_0(x, y)$ specifies the initial values. It is not hard to see from this solution that, *provided* $dv_y/dx \neq 0$, the radial derivative, $\partial f/\partial x$ grows unboundedly in time. This indicates that although the total 'energy' defined by $E(t) = \iint f^2\,dx\,dy$, is indeed a constant of the motion in this diffusionless system, the 'enstrophy', defined by, $H = \iint[(\partial f/\partial x)^2 + (\partial f/\partial y)^2]\,dx\,dy$ grows unboundedly in time, so long as the advection velocity v_y is *non-uniform* (i.e. sheared in x). This immediately indicates that sheared advection has the property of transporting energy in wave number space to higher k_x (i.e. shorter radial wavelengths). This is a form of 'direct' cascade, whereby energy from low k_x is transferred to high mode

numbers, *conservatively*. In physical space, an initially smooth (in x) function which varies in y, develops at later times, highly oscillatory 'wrinkles' or 'corrugations' in the radial direction, *transverse* to the advecting flow.

In these circumstances, we can see immediately that the situation with $\nu \equiv 0$ will be *fundamentally* different to that in which ν is extremely *small but finite*. The appropriate non-dimensional measure of the relative importance of the advection to diffusion is the so-called 'Péclet' number, $Pe = v_y' L_x^2/\nu$. This non-dimensional measure of the relative importance of sheared advection to diffusion is exactly analogous to the well-known Reynolds number, which occurs naturally in problems involving advective–viscous transport of momentum. In the following we shall use both Péclet and Reynolds numbers interchangeably. It is useful to note that it is the *vorticity* (equivalently, radial shear) in the advection that is responsible for the effect in question, since any unsheared flow can always be removed by a Galilean transformation, and cannot therefore be responsible for physical effects other than a trivial, real frequency change. For this reason, the Péclet number defined above contains the vorticity (or shearing rate) rather than the advection velocity itself.

Thus, ν 'small' corresponds to very large values of Pe. The situation described above occurs when $Pe = \infty$. If Pe is large, even if the diffusion term is *initially* negligible (when the energy resides in the low-k_x part of the spectrum and f is relatively smooth as a function of x), for large times, it is *never* negligible, since the high-k_x behaviour is totally dominated by diffusion. We say that at high Péclet numbers the diffusion *cuts off* the direct cascade and leads to entropy/heat production. This last statement is the content of (2), which in fact describes the energy decay of the system. The negative of the right-hand side can be take as the rate of entropy production in the system. As ν tends to zero, this term does *not* go to zero! Rather, the cascade in k_x tends to be cut off at higher and higher values. The cut off values of k_x denoted by, $k_x^{\max}$ are obviously $\simeq \nu^{-1/2}$. The dissipation rate becomes asymptotically (i.e. as $Pe \to \infty$) *independent* of ν. This type of asymptotic behaviour is typical in both fluids and plasmas. Thus diffusion constitutes, in the limit of high Péclet numbers, a *singular* perturbation on the sheared advective transport characterizing the large-scale motions. The energy is fed into the system typically at low to medium wave numbers (constituting the so-called *inertial subrange*), whilst the dissipation takes place at around the cut-off at high k_x.

A second interesting feature revealed by (5) is the following: it is clear that the Fourier transform of f with respect to t gives a *continuous* spectrum in frequency (see also [7] for other examples). Thus, for each mode number m, the frequency of the mode, ω, varies with the radial location x according to the 'local' dispersion relation, $\omega(x) = v_y(x)k_y$. Furthermore, the 'eigenfunction' corresponding to such a continuum eigenvalue is a singular (i.e. non-normalizable), generalized function. These singular eigenfunctions are obtained exactly as in the well-known Van Kampen–Case analysis from (4):

$$i[v_y(x)k_y - \omega]\hat{\phi}_{m,\omega}(x) = 1$$

$$\hat{\phi}_m(\omega) = \frac{i}{[\omega - v_y(x)k_y]}. \tag{6}$$

It is also evident that although f itself does not 'decay', just as in the Van Kampen–Case theory of Landau damping, any integral over f with respect to x would be

'continuum damped'. This is directly a result of the 'phase mixing' due to the transverse advection. Indeed, this simple advection–diffusion model encapsulates all forms of continuum damping, be it in the theory of Alfvén waves, kinetic theory or radiative damping in quantum theory. It shows quite explicitly that phase mixing due to the advection operator rather than any 'wave–particle resonance' is at the heart of linear collisionless damping by a continuum of Van Kampen–Case modes, as originally pointed out by Van Kampen himself [9].

In the light of the fact that the diffusion term is a singular perturbation on the advection operator, the question naturally arises as to how the spectrum behaves when the Péclet number is large, but finite. It turns out that there are two distinct and rather different resolutions of this question depending on the detailed physics.

First, let us consider an apparently 'artificial' problem where the diffusivity ν is taken to be purely imaginary! Thus we set, $\nu = i\mu$, where μ is a real number with dimensions of diffusivity. Equation (4) leads (upon introducing the harmonic time dependence, $\hat{f}_m = \hat{\phi}\exp(-i\omega t)$) to the Sturm–Liouville problem in x with homogeneous boundary conditions:

$$\mu\frac{d^2\hat{\phi}}{dx^2} = \left[\mu k_y^2 + k_y v_y(x) - \omega\right]\hat{\phi}. \tag{7}$$

An immediate consequence is that, irrespective of the size or sign of μ (so long as it is a real, non-zero number), all the eigenvalues ω *must* be real and form a discrete spectrum. Thus, the continuum of the pure advection problem is 'resolved' into a *discretum* by the imaginary diffusion term. Of course, in this case, the meaning of f is not clear as it is a complex quantity. The advection–diffusion equation with imaginary diffusivity can serve as a paradigm for a *time-reversible* system in which a purely *reactive*, *entropy-preserving* effect occurs as a singular perturbation on the advection of a complex scalar. Although at first sight this looks far removed from classical physics, in actual fact, this is a paradigm for 'collisionless tearing' which occurs when the non-ideal effect in Ohm's law is *not* resistivity but electron inertia, which provides a purely non-dissipative, reactive effect leading to tearing, within a two-fluid context. Such an effect would be expected, by considerations similar to those above, to resolve the Alfvén continuum into a closely spaced, non-decaying 'discretum'.

Next, we consider the second, more 'natural' type of resolution of the continuum by real diffusion, which is an irreversible, entropy-producing process. Thus retaining the original ν with the stipulation that it is real and positive, the eigenvalue problem for ϕ becomes in this case,

$$\frac{d^2\hat{\phi}}{dx^2} = \frac{\nu k_y^2 + i\left[k_y v_y(x) - \omega\right]}{\nu}\hat{\phi}. \tag{8}$$

In all generic cases, this constitutes a non-self-adjoint problem for the complex eigenfunction ϕ and the eigenvalue ω, for given $\nu, k_y, v_y(x)$. However, we can immediately show that the eigenvalues ω *must* form a discrete spectrum, and furthermore, must lie in the lower half ω-plane. These facts are simple consequences of (2) and the observation that any solution of (8) must be square integrable in $0 \le x \le L_x$, as the potential has no singularities in this interval for any ω. When ν becomes small (i.e. the Péclet number is large) (8) could be attacked by the complex WKB method for arbitrary but analytic $v_y(x)$. Alternatively, to provide insight, $v_y(x)$ may be approximated by piecewise linear or quadratic functions, and the

equation solved exactly in each approximating interval by Airy/Weber functions and the eigenvalues calculated numerically. A complementary approach to this semi-analytic procedure would be to solve the equation numerically and determine the eigenvalues for arbitrary ν, k_y for the given $v_y(x)$. It is this last approach that will be the main focus of this paper. Finally, one could directly simulate the *initial-value problem* numerically and by suitable 'filtering' procedures, extract the relevant eigenfunctions and eigenvalues. This 'time-marching' approach is analogous to the Green function method of Titchmarsh [10], which will now be described. It is the most general method applicable in principle to all non-self-adjoint problems.

Let us return to the governing equation, (4) for the mode-amplitude, $\hat{f}_m(x,t)$. We attempt to solve the initial-boundary value problem posed for this partial differential equation (PDE) in (x,t) for given m, by taking Laplace transforms. We note that the relation between Laplace and Fourier transforms is well known, and the use of the Laplace transform in initial-value problems follows Landau's approach to the Vlasov problem, and is merely one of convenience.

Henceforth, we simply suppress the suffix m, although this appears as a parameter in the equation. Ultimately the complete solution must be obtained by a Fourier synthesis of all the m-modes. We take the Laplace transform of $\hat{f}$ with respect to t:

$$\hat{F}(x,p) = \int_0^\infty \hat{f} \exp(-pt)\, dt. \tag{9}$$

The transform function $\hat{F}$ then satisfies the *inhomogeneous ordinary differential equation*:

$$p\hat{F} - \hat{h}(x) = -ik_y v_y(x)\hat{F} - \nu k_y^2 \hat{F} + \nu \frac{d^2\hat{F}}{dx^2}, \tag{10}$$

where $\hat{h}(x)$ is the specified 'initial' amplitude. This equation is to be solved for $\hat{F}$, subject to (say) homogeneous boundary conditions at $x = 0, L_x$, where p is treated as an arbitrary complex parameter. From the preceding analysis, it is easily established that $\hat{F}$ is an analytic function of the complex variable p and has no singularities in the (finite) right half p-plane. It is well known that the solution of (10) may be represented in the form,

$$\hat{F}(x,p) = \int_0^{L_x} \Gamma(x,x',p)\, \hat{h}(x')\, dx', \tag{11}$$

where the Green function, $\Gamma(x,x',p)$ is also analytic in the complex variable p and satisfies

$$p\Gamma(x,z) - \delta(x-z) = -ik_y v_y(x)\Gamma(x,z) - \nu k_y^2 \Gamma(x,z) + \nu \frac{\partial^2 \Gamma}{\partial x^2}. \tag{12}$$

In this equation, $\delta(x-z)$ is Dirac's delta function. Since the inverse Laplace transform of Γ yields a contour integral over the complex variable p, it follows that the singularities of Γ, regarded as an analytic function of p, determine the behaviour in time of $\hat{f}$. It readily follows from standard theorems in the theory of second-order linear differential equations with analytic coefficients and reasonably smooth functions $v_y(x)$ that $\Gamma(x,z,p)$ can only have poles in the left half (i.e. $\mathrm{re}(p) < 0$) p-plane; no other type of singularity is allowed for real, positive ν, however small it may be. From this fact we deduce the following consequences. The Bromwich

contour integral,

$$\hat{G}(x,z,t) = \oint \frac{dp}{2\pi i}\,\Gamma(x,z,p)\,\exp(pt) \tag{13}$$

may be taken, for $t<0$ along the imaginary p-axis and closed by a semi-circular contour in the right half-plane. The value is, of course zero, indicating consistency with the causality principle built into the Laplace transform. For $t>0$, the contour is closed in the left half-plane and can be written as a sum of contributions over the poles of Γ. As $t\to 0+$, we obtain the 'spectral representation' or the eigenvalue expansion of the delta function. It is remarkable that this method works with essentially no change whether ν is real or complex (with a positive real part). Note, however, that only in the special case when ν is pure imaginary do we obtain a classical, Hermitian, Sturm–Liouville operator.

The above construction will be applied in simplified forms in the following to reveal the intricate and non-trivial spectra associated with the advection–diffusion equation. Instead of calculating the Green function and locating its poles and residues in the left half p-plane, we will directly solve the eigenvalue problem with $p=-i\omega$. Let us also note that the method is also applicable, as it stands, when we include *radial* advection terms of the form, $\frac{\partial}{\partial x}[v_x(x)\hat{f}]$, subject only to the proviso that there should not be any y dependence in the radial advection component, v_x. If this requirement is not satisfied, variables do not separate and Fourier analysis in y does not help.

3. Analytical and numerical solutions of the eigenvalue problem

Let us set, without loss of generality, for convenience in what follows, $L_y=2\pi, k_y=im, v_y(x)=V(x), \lambda=\omega+\nu m^2$. The eigenvalue problem treated in this paper amounts to solving the differential equation

$$\nu f''(x) + i[\lambda - mV(x)]f(x) = 0. \tag{14}$$

This has no general analytic solution for arbitrary velocity profiles, $V(x)$. However, for some specific profiles solutions can be found. These involve transcendental functions that require calculation of the eigenvalues by a suitable numerical method. We shall analyse three cases of the velocity profile $V(x)$ for which an analytic solution is possible: linear, parabolic and sinusoidal velocity profiles.

We first consider the case of a linear velocity profile, $V(x)=\Omega x$ which has uniform shear/vorticity. This is the simplest case, the solution being given by a linear combination of Airy functions. Making the substitution

$$z = i\frac{(\lambda - m\Omega x)}{(\nu m^2\Omega^2)^{1/3}}$$

reduces (14) to Airy's equation:

$$\frac{d^2 f(z)}{dz^2} = z f(z).$$

The solutions of this are expressible in the form

$$f(z) = C_1\,\mathrm{Ai}(z) + C_2\,\mathrm{Bi}(z), \tag{15}$$

where $\mathrm{Ai}(z)$ and $\mathrm{Bi}(z)$ are the Airy functions [11], and C_1 and C_2 are integration constants, which can be determined using the boundary conditions. Eigenvalues

can then be obtained in a 'semi-analytical' manner: given that any multiple of the solution is itself a solution (the equation is linear and homogeneous), we can set one of the integration constants to unity and determine the remaining constant using one of the boundary conditions. The other boundary condition then gives us an equation to which a root-finding method can be applied, hence determining the eigenvalues.

It is useful to observe that Airy functions can also be used whenever $V(x)$ is a *piecewise* linear function of x. The solutions in different regions have to be 'matched' at the points where the profile slope changes. The matching constants satisfy a linear homogeneous system, the determinant of which yields a transcendental equation for the eigenvalue, which requires a numerical solution technique (e.g. Newton–Raphson or interval bisection). This model is useful for simulating irregular (but continuous) advection velocity profiles which are well approximated by piecewise linear functions.

Next, we consider a velocity profile of the type

$$mV(x) = ax^2 + bx \tag{16}$$

where a and b are constants. The transverse advection–diffusion equation then reduces to

$$\frac{d^2f}{dx^2} + \frac{i}{\nu}\lambda f - \frac{i}{\nu}(ax^2 + bx)f = 0. \tag{17}$$

A simple algebraic reduction then leads to the Weber equation [11]. We now proceed in the usual way, by expressing the solution $f(x)$ in the form,

$$f(x) = u(x)\exp\left(-\frac{1}{2}\sqrt{\frac{i}{a\nu}}y^2\right)$$

and again changing the variable to $t = y^2$. After some manipulation we obtain

$$t\frac{d^2u}{dt^2} + \left(\frac{1}{2} - \sqrt{\frac{i}{a\nu}}t\right)\frac{du}{dt} + \frac{1}{4}\left[\frac{i}{a\nu}\left(\lambda + \frac{b^2}{4a}\right) - \sqrt{\frac{i}{a\nu}}\right]u = 0.$$

The solution to the preceding equation can be readily obtained in terms of confluent hypergeometric functions, ${}_1F_1$ (see [11]):

$$u(t) = {}_1F_1\left\{\frac{1}{4}\left[1 - \sqrt{\frac{i}{a\nu}}\left(\lambda + \frac{b^2}{4a}\right)\right], \frac{1}{2}; \sqrt{\frac{i}{a\nu}}t\right\}A$$
$$+ {}_1F_1\left\{\frac{1}{4}\left[3 - \sqrt{\frac{i}{a\nu}}\left(\lambda + \frac{b^2}{4a}\right)\right], \frac{3}{2}; \sqrt{\frac{i}{a\nu}}t\right\}B\sqrt{t},$$

where A and B are integration constants.

Note that the original boundary conditions $f(0) = f(1) = 0$ now become $u(b^2/4a) = u((\sqrt{a} + b/2\sqrt{a})^2) = 0$.

Another interesting case of a radially oscillatory advection velocity profile is of relevance in applications [5, 6]. Thus, consider a velocity profile, $mV(x) = k\sin(p\pi x)$. The transverse advection–diffusion equation becomes

$$\frac{d^2f}{dx^2} + \frac{i}{\nu}\left[\lambda - k\sin(p\pi x)\right]f = 0.$$

We now apply the trigonometric relation $\sin(p\pi x) = \cos(\frac{\pi}{2} - p\pi x)$ and make the change of variable $y = \frac{\pi}{4} - p\frac{\pi}{2}x$. The above equation then becomes

$$\frac{d^2 f}{dy^2} + \frac{4}{(p\pi)^2}\frac{i}{\nu}\left[\lambda - k\cos(2y)\right] f = 0$$

and this is just the well-known Mathieu equation, for which the solution is given in terms of Mathieu functions [11], Mc and Ms:

$$f(y) = A\,Mc\left(\frac{4i\lambda}{p^2\pi^2\nu}, -\frac{2ik}{p^2\pi^2\nu}, y\right) + B\,Ms\left(\frac{4i\lambda}{p^2\pi^2\nu}, -\frac{2ik}{p^2\pi^2\nu}, y\right)$$

and A and B are integration constants. Eigenvalues can be calculated in the same semi-analytical way as described above, noting that the boundary conditions are now given by $f(\frac{\pi}{4}) = f(\frac{\pi}{4} - p\frac{\pi}{2}) = 0$.

We briefly describe the numerical technique used to obtain discrete spectra. The shooting method is employed. This involves the specification of the values of the solution and its derivative at one of the boundaries (the left-hand one, for instance), $f(0)$ and $f'(0)$ are specified, respectively. Then, using the chosen propagation scheme (a suitable finite-difference solver of the initial-value problem) and an initial guess for the eigenvalue λ, the solution can be calculated up to the right-hand boundary, $f(1, \lambda)$. Newton's method, applied to the equation $f(1, \lambda) = 0$, can then be used to converge on the eigenvalue. The iteration formula is given by

$$\lambda_{j+1} = \lambda_j - \frac{f(1, \lambda)}{(\partial f/\partial\lambda)|_{x=1}}.$$

λ_{j+1} is now the new trial value, and a new solution, $f(1, \lambda_{j+1})$ can be calculated. The method can also be varied by starting from both boundaries and imposing 'continuity' of the solution and its derivative at an *interior* point which is judiciously chosen. This is sometimes a better practice than shooting from one boundary. The iterations are continued until a convergence criterion such as $|f(1, \lambda)| < \varepsilon$, where ε is the desired precision, is satisfied.

In principle, for more complex problems, a judicious combination of numerical and WKB-type asymptotic methods will be needed, especially when R becomes very large, as it does in physically realistic problems. The code allows the user to specify an initial guess matrix, of variable size. The bigger the number of initial guesses the more likely it is that all the eigenvalues will be found. Also, increasing the size of the matrix allows for a choice of a smaller number of iterations on which Newton's method is supposed to converge. That is, good initial guesses will lead to faster convergence, hence saving computing time in iterations that take too long to converge, if at all, for the bad guesses.

We now present the results obtained with the code. Where possible, a comparison with analytical solutions is carried out; in all cases excellent agreement is obtained. We first consider profiles of the form $V = kx$, where, k has been set to 10.

We note that the parameter of relevance is the Reynolds (or Péclet, as noted in the introduction) number, $R = L_y^2 V'/\nu$. Note that since $L_x = 1$ in this section, the length used is L_y. It is merely convention as to which length is employed in the definition. Furthermore, it is immaterial physically which parameter (ν or V') is fixed as long as the other one varies. The eigenvalue spectrum found has the following properties.

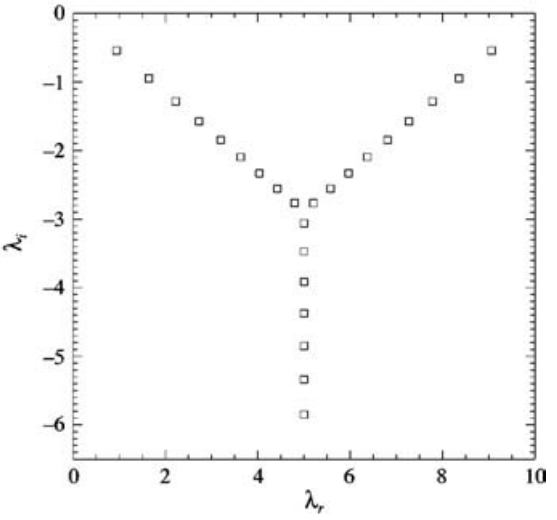

Figure 1. Eigenvalue spectrum for the velocity profile $V(x) = 10x$ and $\nu = 0.001$.

(1) It is discrete and has a Y shape which is independent of the value of R. This means that no matter how *small the diffusivity*, provided it is non-vanishing, the spectral distribution has an invariant shape, although evidently individual eigenvalues will move about in the complex plane. It is essential to note that the spectral distribution does *not* continuously tend to a subset of the real line (i.e. to the continuous spectrum for the purely advective equation).

(2) The density of the eigenvalues increases as $R \to \infty$.

(3) The three branches of the spectrum form a 120° angle with each other. Figures 1–3 illustrate these points.

The results obtained with the code are in complete agreement with the analytic solution given earlier. Applying Newton's method to the analytical solution has allowed us to determine the eigenvalues for values of the diffusivity as low as $\nu = 10^{-8}$ ($R = 10^9$). This is because in this method we do not have to deal with accuracy problems arising from insufficiently small space steps. Figure 3 shows two examples of eigenvalue structures obtained in this manner.

It is perhaps surprising that a continuous transition in the spectrum from the case $\nu = 0$ (in this case, the spectrum is 'continuous' along the portion of the real axis corresponding to the range of $mV(x)$, as pointed out in Sec. 2) to very small values of ν (that is, from ideal to dissipative) does not occur. We note that an arbitrarily small amount of diffusivity is sufficient to break the frozen flux constraint, which gives rise to qualitatively very different behaviour of the system. The example also demonstrates the fact that modes with $\lambda_r \simeq 5$ are strongly damped (i.e. $-\lambda_i \geq 3$) even though $\nu \to 0$.

This discontinuous transition is not a new result and has been addressed in papers by Lortz and Spies [12] and Dewar and Davies [13], in connection with the corresponding phenomenon in ideal magnetohydrodynamics (MHD). The mathematical explanation for this 'paradox' (i.e. that the ideal and dissipative spectral distributions have a different morphology in the limit as the diffusivity goes to zero) is due

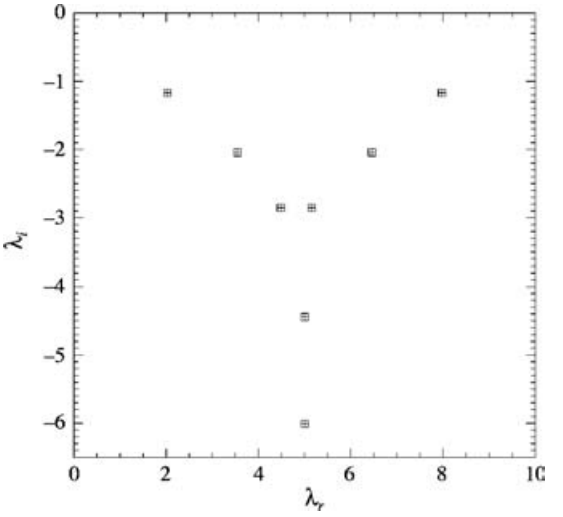

Figure 2. Same as in the previous graph but with $\nu = 0.01$. Squares denote points calculated numerically, crosses denote semi-analytical results. Notice the convergence of the branches at the same point as before.

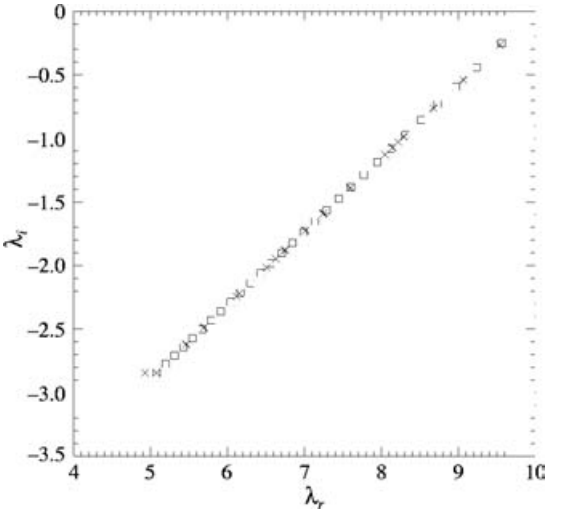

Figure 3. Semi-analytical solutions for the same linear profile. Squares denote solutions with $R = 10^5$, crosses denote $R = 10^9$ results. Both spectra are incomplete; again notice the exact overlap of the overall structures, showing the independence of the value of ν; also, an increase in the eigenvalue density is clear.

to the fact that diffusion is a *parabolic singular perturbation* of the advective (i.e. *hyperbolic*) equation. The examples given earlier elucidate this phenomenon clearly, and show that sheared advective flows, by their nature, tend to cascade energy conservatively to very high transverse wave numbers where even tiny amounts of dissipation can result in damping. If the system without advection (but has small diffusion) is *unstable*, the addition of advection effectively increases the damping

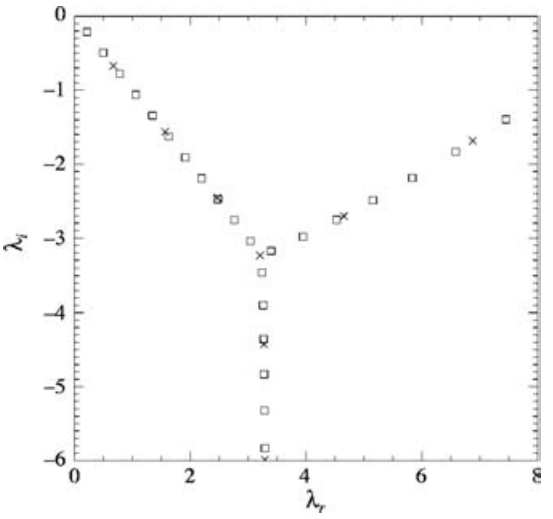

Figure 4. Eigenvalue spectrum for the parabolic velocity profile $V(x) = 10x^2$ and $\nu = 0.001$ (squares) and $\nu = 0.01$ (crosses). The overall structure is also independent of the value of the diffusivity.

rate to $\nu^{1/3}\Omega^{2/3}$ from being merely proportional to ν, where $\Omega \simeq V'$. This purely *linear* mechanism is highly likely to be implicated in the suppression of turbulence by zonal flows [1, 4–6, 18].

It should be stated that for large Reynolds numbers, it becomes difficult to find the eigenvalues with the computer code. This is due to two reasons.

(1) As the value of R increases, the variations in the solution, $f(x)$ increase too. Hence, the space step has to be made increasingly smaller to cope with this, until it becomes computationally impractical to solve the equations.

(2) The density of the eigenvalues increases as R increases. At a certain point they will be so close to each other that Newton's method has difficulty in maintaining convergence. A more robust technique such as interval-halving can then be used, with some care in the choice of the interval, in judicious combination with an analytic asymptotic expansion for large R.

In the case of a parabolic profile $mV = kx^2$, where k has again been set to 10, the spectrum was found to have the same general properties as the linear case (invariance for the value of the diffusivity and increase in the density of the eigenvalues as $R \to \infty$), except that now the Y shape is no longer symmetrical. The left arm now makes a 45° angle with the horizontal, thus implying that eigenvalues in this region have symmetric real and imaginary parts. Figure 4 illustrates this for two different values of the diffusivity. Comparison with semi-analytical results again yields excellent agreement, as can be seen in Fig. 5.

Next, we consider a purely sinusoidal profile, $V(x) = k\sin(n\pi x)$, where n is some integer and k is a constant. An analytical solution is possible, as shown earlier. The agreement between numerical and semi-analytical results is again found to be entirely satisfactory. In this case, degeneracy in the eigenfunctions (i.e. different eigenfunctions associated with the same eigenvalue) is to be expected due to symmetry considerations. The domain is geometrically invariant upon a 180°

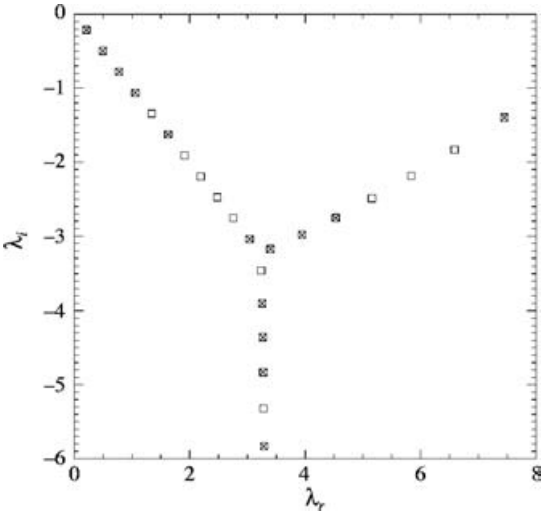

Figure 5. Numerically obtained eigenvalues (squares) versus some semi-analytic results (crosses): very good agreement can be observed.

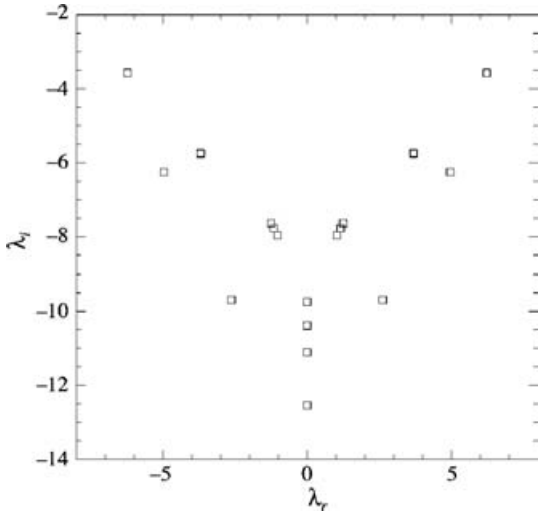

Figure 6. Eigenvalue spectrum for the sinusoidal profile $V(x) = 10\sin(8\pi x)$. More than one eigenfunction corresponds to the same eigenvalue.

rotation, making this situation similar to the cubic box potential for the Schrödinger equation, where degeneracy is known to occur. An example can be seen in Fig. 6.

The introduction of a linear contribution to the profile, however small, immediately destroys this symmetry, thus removing degeneracy. It is then more interesting to analyse profiles where this undesired effect has been eliminated, of the form:

$$V(x) = k_1 x + k_2 \sin(n\pi x). \tag{18}$$

One question is how the transition from the linear profile to that given in (18)

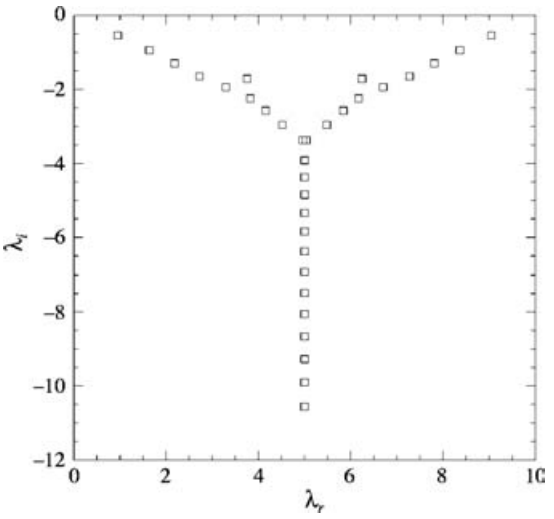

Figure 7. Spectrum for $V(x) = 10x + 0.01\sin(8\pi x)$. Note how the Y shape from the purely linear profile is deforming subtly.

occurs. If k_2 is made very small, then we can think of the sinusoidal component in (18) as a small perturbation to the unperturbed operator

$$L_0 = i\nu\frac{d^2}{dx^2} + k_1 x.$$

As seen earlier, this operator has a point spectrum. A standard theorem due to Kato [14] can be used to explain the transition. According to this theorem, a point spectrum (i.e. discrete) of an unperturbed operator L_0 changes continuously into the point spectrum of a regularly perturbed operator $L = L_0 + \varepsilon L_1$ as the perturbation L_1 is switched on. Figures 7 and 8 illustrate this continuous transition. The same reasoning obviously applies in the reciprocal case of perturbing the sinusoidal potential with a linear one.

By a 'jet' profile we mean a velocity field that is zero everywhere except in a small region of the domain, where it assumes a high value (typically, a Reynolds number $R = 10^4$ is sufficient to validate all the following conclusions). Physically, this kind of profile can be driven by both turbulent Reynolds and Lorentz forces/stresses and corrugations in the ion pressure gradient. In the case of electron physics, current gradients and dynamo effects produce similar changes in advective (i.e. electron inertial) terms. We have studied the effect of a profile composed of two of these jets, i.e.

$$V(x) = \begin{cases} V_{01}, & x_{01} - \delta < x < x_{01} + \delta \\ V_{02}, & x_{02} - \delta < x < x_{02} + \delta, \end{cases}$$

where V_{01} and V_{02} are the constant heights of the jets, x_{01} and x_{02} their centres and 2δ the total width of a jet (assumed to be the same for both jets). Elsewhere $V(x) = 0$. Given that the profile is either zero or constant, the solution to the governing advection–diffusion equation is trivial in each sub-region of the domain. Eigenvalues can thus be obtained by matching solutions from the different regions and using the boundary conditions. Very good agreement was obtained between numerical and analytic eigenvalues.

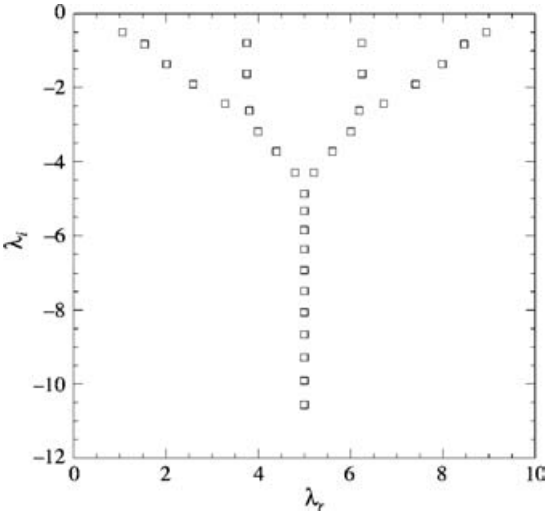

Figure 8. Compare with Fig. 7. As the sinusoidal contribution is increased so that $k_2 = 0.1$, the Y shape becomes more deformed.

The main results may be summarized as follows.

(1) The spectrum has as many branches as the number of regions into which the domain is divided. Thus, for instance, if we are considering the double-jet case, the spectrum will have a three-arm structure.

(2) Geometric degeneracy occurs if the domain is invariant under rotation/reflection. For example, in the case of a double-jet profile, there will be degeneracy if $V_{01} = V_{02}$ and jets are equally spaced from the boundaries of the domain (say, for instance, $x_{01} = 0.35$ and $x_{02} = 0.65$). This degeneracy translates itself in the eigenspectrum as overlapping arms. In this situation there are two obvious ways to remove the degeneracy: either make $V_{01} \neq V_{02}$ or make the distances from the centres of the jets to the boundary walls different. In Fig. 9 we show a situation where degeneracy has been removed by displacing one of the jets.

(3) Different regions of the domain are isolated from each other, implying that eigenfunctions will approach zero values near the jets, as can be seen in Fig. 10. For high enough Reynolds numbers ($R = 10^5$ is already sufficient) eigenfunctions will only exist in one of the three regions in which the jets divide the domain. We have thus found that this kind of velocity profile confines the eigenfunctions in the regions between the jets. Each branch of the eigenspectrum denotes one of these regions.

Figures 11–14 show the eigenvalues and eigenfunctions for two double-jet cases, in which the jets are symmetrically placed but are in 'opposite' directions, i.e. $V_{01} = -V_{02}$. Figure 11 shows how increasing the height of the jets causes the real components of the eigenvalues to tend toward zero, while Figs 12–14 graphically demonstrate the isolation of the eigenfunctions within the three regions divided by the jets.

The confinement of the eigenfunctions is an interesting result and should be of importance in the limiting of radial correlations and propagation effects associated

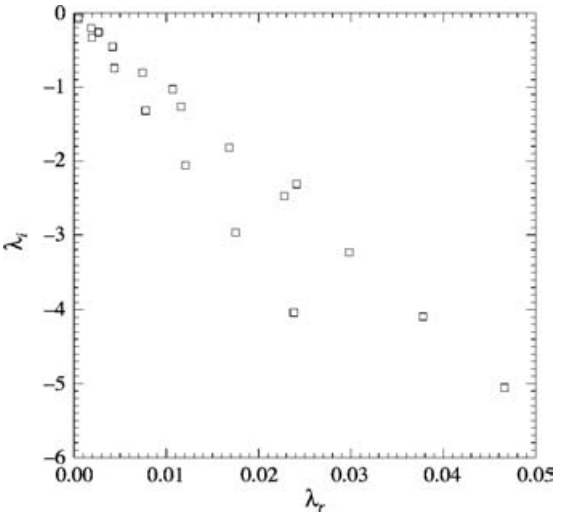

Figure 9. Spectrum for a double-jet profile: $V_{01} = V_{02} = 500; x_{01} = 0.35; x_{02} = 0.80;$ $\delta = 0.005$. Three independent branches can be seen: degeneracy has been removed by breaking symmetry through displacement of one of the jets.

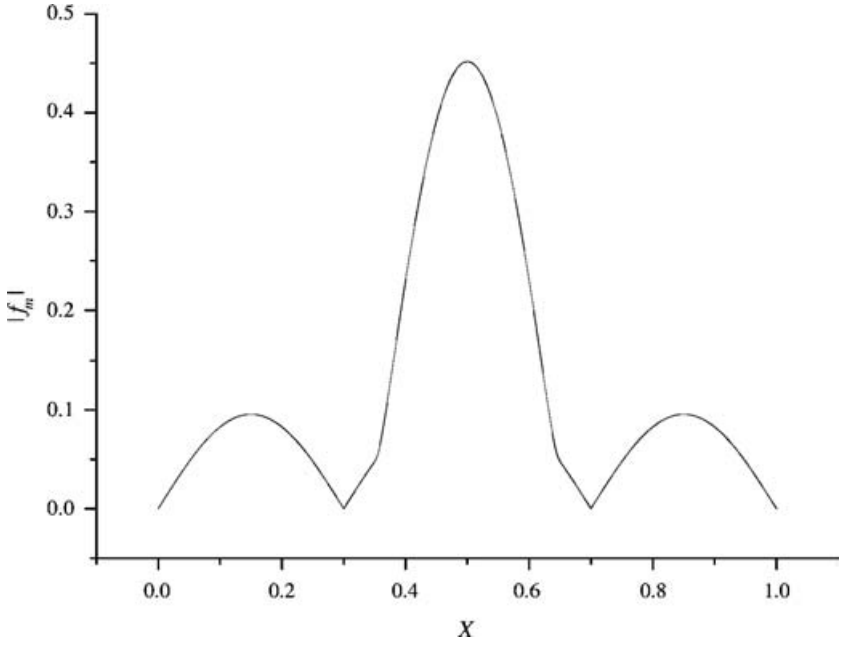

Figure 10. Lowest-order mode for a $R = 10^4$ double-jet velocity profile. The jets are placed at $x_{01} = 0.35; x_{02} = 0.65$, with width $\delta = 0.01$. The eigenfunction has nearly zero values in the highly sheared vicinity of the jets, meaning that the three regions are isolated.

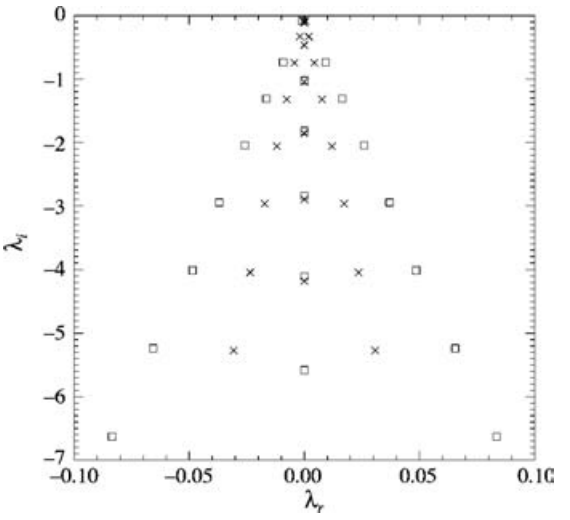

Figure 11. Eigenvalues for two different double-jet profiles. Squares denote the results for $V_{01} = -V_{02} = 100$, while crosses denote the results for $V_{01} = -V_{02} = 500$. It can be seen how increasing the height of the jets makes $\lambda_r \to 0$.

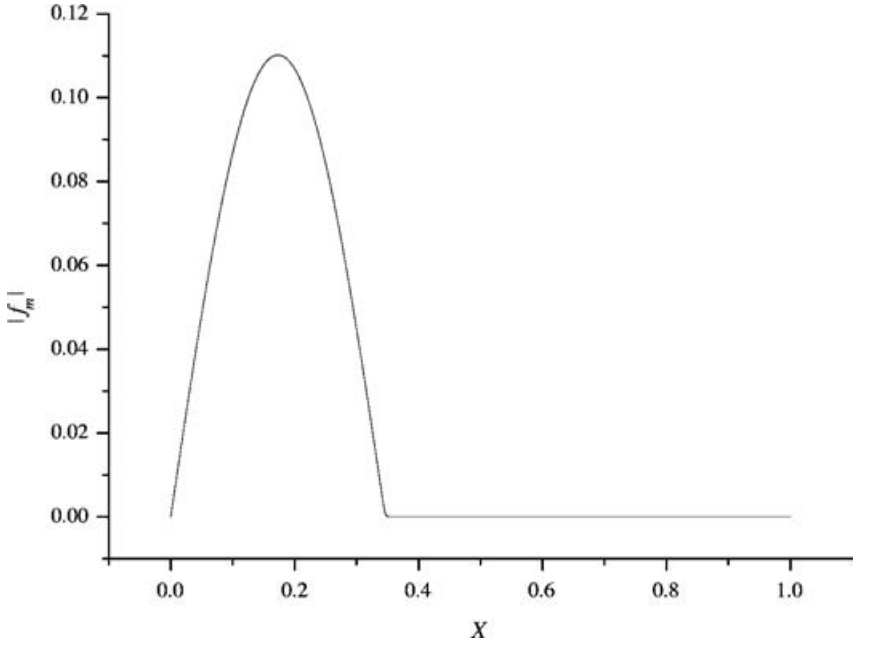

Figure 12. Lowest eigenfunction of the left-hand arm for a double-jet profile with $V_{01} = -V_{02} = 500$. Complete confinement of the eigenfunction is observed.

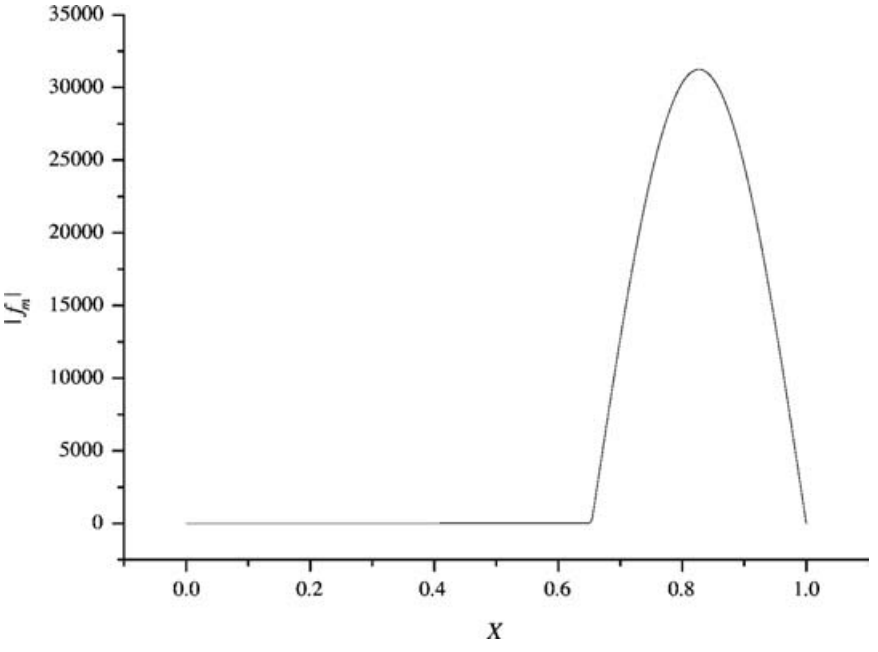

Figure 13. Same as above for the right-hand arm.

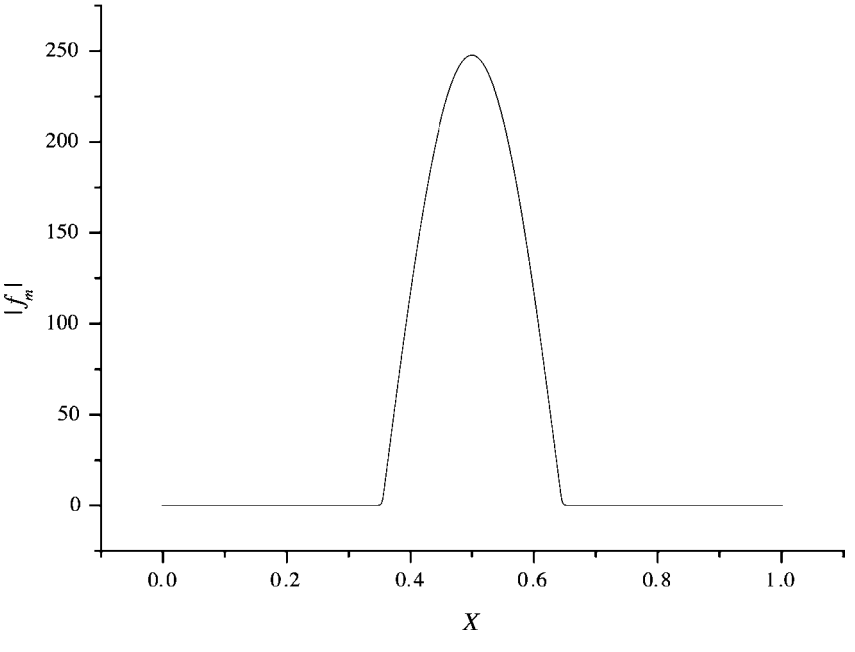

Figure 14. Same as above but for the central arm.

with the turbulence. Hence, it may alter the turbulent transport. Results are obviously generalizable for an arbitrary number of jets. It should be noted that this type of 'ghettoization' of transported scalars by advection–diffusion equations was already foreshadowed in an astrophysical context in an earlier investigation by Parker and one of the authors [8].

4. Solutions of the initial-value problem for the advection–diffusion equation: the evolutionary approach

Next, we describe the CADENCE code which treats advection–diffusion equations such as (1) using parallel processing clusters by solving the appropriate initial-boundary problem. For simplicity, we only consider the case of purely radial diffusion, denoting the diffusivity in this section by D. The code solves problems in three spatial dimensions. As before, the x-direction corresponds to the 'radial' direction, whilst the y, z-directions correspond to 'poloidal' and 'toroidal' directions in a tokamak [5].

The general form of the equation solved by CADENCE is a variation on (1):

$$\frac{\partial f}{\partial t} + v_y \frac{\partial f}{\partial y} + v_z \frac{\partial f}{\partial z} + \frac{\partial}{\partial x}(v_x f) = \frac{\partial}{\partial x}\left(D \frac{\partial f}{\partial x}\right) + gf + S. \tag{19}$$

Here, a second transverse advection term is present, and there are also 'radial' advection (v_x), source (S) and growth rate (g) terms. The coefficients of all the terms are (in general) complex-valued functions of x, y and z.

Thus, CADENCE solves for $f = f(x, y, z, t)$ in the domain (using a non-dimensional radial coordinate) $0 \leq x \leq 1$, $0 \leq y, z \leq 2\pi$, with f periodic in y and z such that $f(x, y, z, t) = f(x, y + 2\pi, z, t)$ and $f(x, y, z, t) = f(x, y, z + 2\pi, t)$. We assume the boundary values $f(x = 0, y, z, t)$, $f(x = 1, y, z, t)$ and the initial condition, $f(x, y, z, t = 0)$ to be given. The function f is evolved in time by forming a finite-difference equation from (19) and re-arranging to produce a tridiagonal matrix equation in f that can be solved very efficiently.

CADENCE was developed as the precursor of a new fully three-dimensional turbulence code for realistic tokamak geometries, which is why the second transverse direction is included in the above equation. A property of tokamak plasmas is that the timescale for transport effects is much longer in the radial direction than in the poloidal and toroidal directions, and this provides a convenient method of parallelizing the code on to a number of processors. The x domain is split into n_p equal sub-domains (these are annuli or layers in the x-direction), one for each of the n_p processors, and each processor solves the partial differential equation in its own sub-domain, passing appropriate values of f to its 'neighbouring' processors after each timestep. Figure 15 shows how the distribution of x elements is arranged; adjacent processors 'overlap' so that they have two common elements, and during the course of the calculation the function values at these points are passed from one processor to the other to ensure continuity in the solution.

For the purposes of this paper, we will use a cut-down version of (19) to demonstrate how CADENCE has been used to provide extra insight into the results from the eigenvalue code described earlier. The two approaches validate each other's findings, but also bring out complementary properties in the advection–diffusion equation. Here, we restrict ourselves to a single transverse direction, exclude radial advection and growth rate terms, and consider typical initial values and boundary

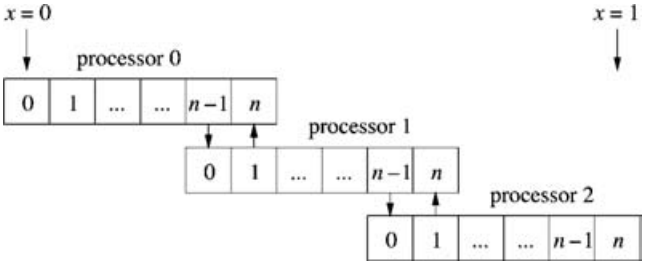

Figure 15. Distribution of x elements between three processors. During each solution cycle the values of f at the elements near the internal boundaries between adjacent processors are passed in the direction indicated. Processor $(k+1)$ evolves f_1 via the solution of the matrix equation and passes the value into f_n on processor k, and processor $(k-1)$ evolves f_{n-1} and passes the value into f_0 on processor k.

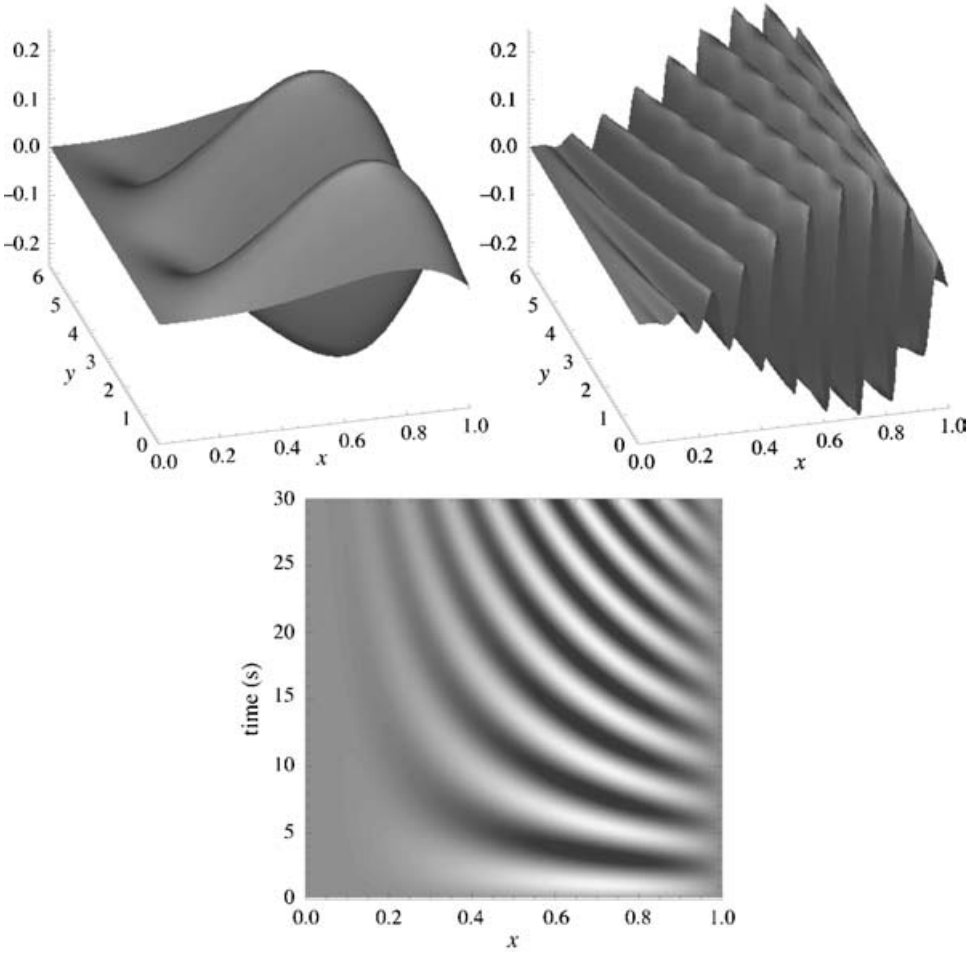

Figure 16. CADENCE calculation of the evolution of a function $f(x, y)$ with transverse advection $v_y(x) = -x$, in the absence of diffusion. The upper left-hand plot is the initial state of f, the upper right-hand plot is f at $t = 30\,\mathrm{s}$, and the lower plot shows the evolution in time of f at a fixed y. The increase in radial wave number k_x is immediately apparent.

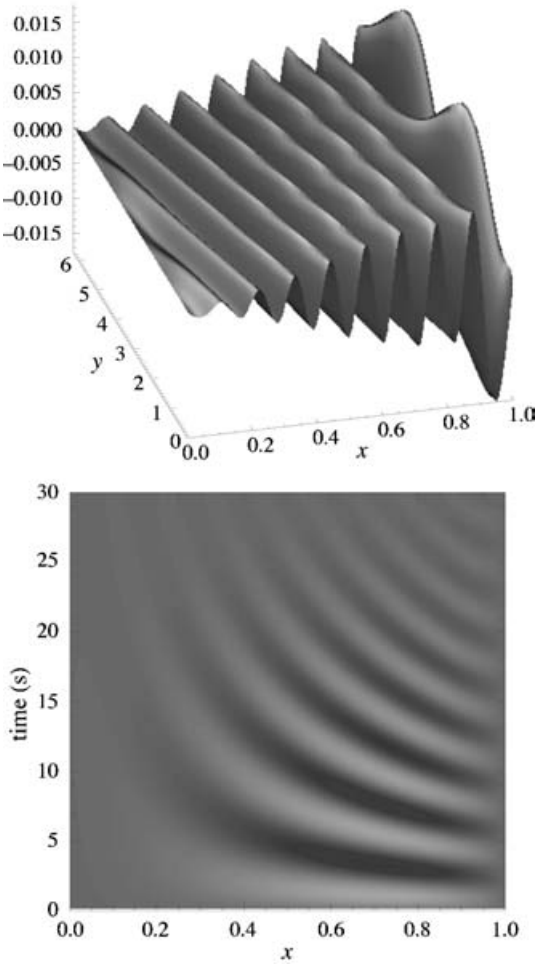

Figure 17. CADENCE calculation of the evolution of the same initial function $f(x, y)$ as in Fig. 16 but with the addition of a small amount of diffusivity, $D = 10^{-4}$. The upper plot is the state of f after $t = 30\,\mathrm{s}$ and the lower plot shows the evolution in time of f at a fixed y. The preferential decay of the high-k_x waves is clear.

conditions given by

$$\begin{aligned} f(x, y, t = 0) &= x^2(1 - x^2)\sin 2y \\ f(x = 0, y, t) &= 0 \\ f(x = 1, y, t) &= 0. \end{aligned} \tag{20}$$

Here, since $L_x = 1$, v_0'/D_0 is the Reynolds/P/'eclet number R, which can take any value. If R is high, advection dominates, whereas, for R low, diffusion dominates.

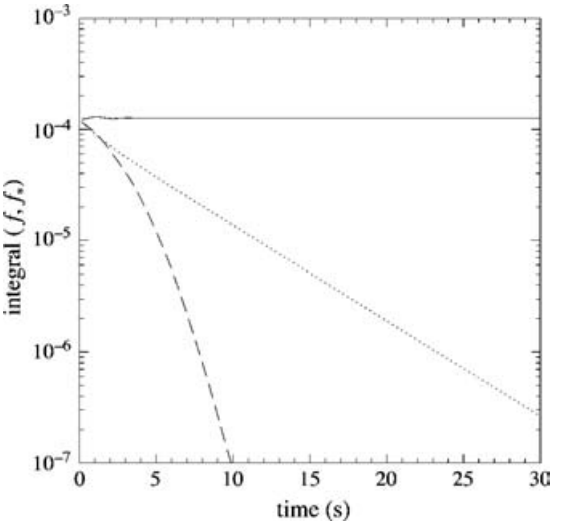

Figure 18. CADENCE calculation showing how the rate of change of total energy $E(t) \equiv \iint f^2\, dx\, dy$ varies for three different cases: (1) advection $v_y = -x$, no diffusion (solid curve); (2) diffusion $D = 10^{-2}$, no advection (dotted curve); (3) both advection $v_y = -x$ and diffusion $D = 10^{-2}$ (dashed curve).

The equation may be solved by expanding $f(x, y, t)$ in a Fourier series with respect to y and then applying the differential equation to each component:

$$f(x, y, t) = \sum_{k=-\infty}^{k=\infty} F_k(x, t) e^{iky} \tag{21}$$

$$\Rightarrow \frac{\partial F_k}{\partial t} = D \frac{\partial^2 F_k}{\partial x^2} - ikv_y F_k + S_k. \tag{22}$$

($S_k = 0$ except for $k = 0$ in our case). This is straightforward to translate into a difference formula, and then into a tridiagonal matrix equation for each k value (i.e. the different F_k do not 'interact' in this linear model). All Fourier transforms are carried out using the fast Fourier transform algorithms.

Figure 16 demonstrates graphically the evolution of the $D = 0$ case described earlier, as calculated by CADENCE. The cascade of energy into higher and higher wave numbers is immediately apparent. The initial function f has a $\sin 2y$ variation, and this is preserved at all x values at all times, but the number of waves in the x-direction rises steadily.

Compare this result with Fig. 17, which introduces a small ($D = 10^{-4}$) diffusivity into an otherwise identical problem. The diffusion, though apparently insignificant, still wins out because of its strong decay of high-k_x waves as predicted earlier. In fact the combination of advection as well as diffusion causes a much faster reduction in the energy $E(t) = \iint f^2\, dx\, dy$ of the system, as shown in Fig. 18, which compares $E(t)$ for the advection-only, diffusion-only and advection + diffusion cases.

In Sec. 3 above, it was pointed out that the eigenvalue code described there has difficulty in finding eigenvalues for small values of D. In contrast, the eigenvalue

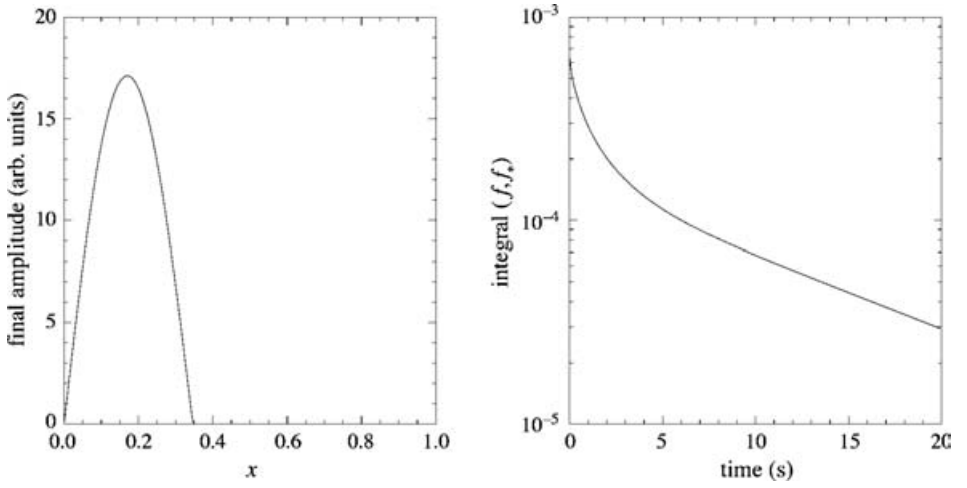

Figure 19. CADENCE calculation of the double-jet case of Fig. 12, showing the confinement of the function by the left-hand jet at $x = 0.35$. The amplitude plot on the left-hand side shows the final eigenfunction, and is the same as that calculated using the eigenvalue code. The integral plot on the right-hand side shows the decay of $E(t)$ with time, and the final gradient gives the eigenvalue as 0.0824, again in agreement with the eigenvalue code.

corresponding to the slowest decaying mode can be found easily using CADENCE, as they are simply evaluated from the gradient of $y(t) = \log E(t)$ (as in Fig. 18) at large t. In this way CADENCE has been used successfully to verify the eigenvalues and the spectra for all of the more complicated cases described earlier. For instance, Fig. 19 shows the final solution of the double-jet run shown in Fig. 12, as calculated by CADENCE. The initial function was a delta function at $x = 0.05$, varying as $\sin y$ in the y-direction. As expected, the initial function spreads out in x, but is confined by the left-hand jet. The slope of the $\log E(t)$ curve tends towards a value of 0.0824, in agreement with the calculation by the eigenvalue code.

5. Discussion and conclusions

In this paper, we have considered a paradigmatic analysis of one of the simplest non-self-adjoint equations, namely the linear advection–diffusion equation. In important special cases, the equation is exactly solvable in terms of well-known functions. It has also been found possible to treat its spectral properties relatively generally using the Green function approach (alternatively called the 'resolvent' method). These analytic techniques are supplemented by an eigenvalue approach and an evolutionary initial-value approach using standard numerical algorithms. These methods apply of course to far more complicated and realistic systems of parabolic differential equations encountered in fluid mechanics and plasma physics.

The key conclusions of our studies are summarized as follows: in the absence of diffusion, purely advecting systems, although conserving energy, can lead to an 'ultraviolet' catastrophe. This manifests itself in a 'direct cascade' where the sheared flows 'phase mix' structures transverse to flows and the energy is transported in radial wave number space to arbitrarily high wave numbers. Spatially the transported property acquires radial 'fine structure' or 'corrugations' [5, 6] seen in much

more general *non-linear* simulations. Purely diffusive systems, on the other hand, imply a simple damping, the rate being directly proportional to the diffusivity. This damping can be very weak when the diffusivity is small and the initial radial variation of the transported property is relatively smooth. What we have sought to demonstrate explicitly is the large increase in the damping by even small diffusivity in the presence of sheared advection transverse to the direction of diffusion. It is easy to see from dimensional arguments alone (also confirmed both by the exact and the numerical solutions) that the damping rate is greatly enhanced by the sheared flow due to the latter's phase mixing capacity. Thus, qualitatively speaking, a small diffusivity ν, in the presence of a shearing rate, Ω is capable of damping at the *hybrid* rate, $\nu^{1/3}\Omega^{2/3}$, namely, far faster than in the absence of sheared flows. This effect is also associated with the fact that the spectra of the purely advective (conservative) systems are not approached uniformly by those of the advection–diffusion system in the limit as the diffusivity tends to zero. This 'paradox' is merely the consequence of the fact that the properties of parabolic systems 'close' to hyperbolic ones do not necessarily reduce to those of the latter. Parabolic effects caused by irreversible diffusion are necessarily singular perturbations and it has long been known in fluid mechanics and elsewhere that the limits are non-uniform. The capacity of sheared advective flows to enhance damping rates may at least be partially responsible for the so-called 'shear flow stabilization' of turbulence studied in several recent works in tokamak physics. That such flows also provide an important route to direct cascades of energy is clearly illustrated by our results.

We have also demonstrated that regions of highly sheared flows can 'confine' or create 'ghettos' in the transport properties. This could be effective in both plasmas and in geophysical/astrophysical situations (e.g. as in [8]) where strong jet-like flows can be created by the turbulence itself. Of course, the considerations extend to effects produced by currents, which are usually flows of the electron fluid. Electron flows can (and do) transport temperature and magnetic flux, and the advection–diffusion equation (albeit in its fully non-linear forms) is ubiquitous in the consideration of such transport properties.

The methods described here can also be applied to *systems* of parabolic equations involving strongly sheared advections such as those encountered in applications [5]. Indeed, if the advection terms change relatively slowly in time compared with the shearing rates themselves, it is possible to define in a meaningful fashion, the 'instantaneous' spectra of the system (with respect to the 'slow' time, of course) and obtain insight into the nature of the evolution. Another well-known application [15] is to purely radial advection interacting with radial diffusion. In this case, the problems are reducible to a Hermitian operator, and variational methods of determining spectra and eigenfunctions become applicable. This type of advection–diffusion equation also has a very important role in plasma transport processes. The interplay of radial advection and diffusion is thought to be intimately linked to the formation and dynamics of 'internal transport barriers' and radial propagation of heat and density pulses in transient experiments conducted on tokamaks [16].

In fluid mechanics, it is well known [17–19] that sheared flows are susceptible to instabilities both in inviscid (cf. the Rayleigh criterion and Kelvin–Helmholtz instability) and in viscous conditions (cf. instabilities of the Orr–Sommerfeld equation at high Reynolds number). These are inherently more complicated problems than those investigated in the present paper for the important dynamical reason that the advected quantity is not a 'passive scalar' but is actually the flow velocity

itself (or the vorticity). The resultant profile–fluctuation interaction can amplify the disturbance in a way that counteracts the tendency of sheared flows to decorrelate transversely oriented eddies and to thereby damp fluctuations. However, it is also well known that simple sheared flows which are actually linearly stable may be *non-linearly destabilized* (i.e. can be subject to 'subcritical bifurcations' or finite-amplitude instabilities). These more complex phenomena have been investigated in detail in many works apart from those cited above. Since our purpose is to understand the effects of advection *per se* and its ability to amplify the effect of dissipative damping by phase mixing and direct cascading to higher wave numbers, the non-linear interactions responsible for subcritical behaviour of shear flow instabilities lie somewhat outside the scope of the present work. Our results do suggest however, that the non-linear shear-flow instabilities could be caused by a competition between the phase-mixing/direct cascade due to sheared advection and the Kelvin–Helmholtz-type instability of flow profiles with strong gradients and/or points of inflection. This tentative conjecture remains to be investigated in detail and firmly established by future analytical and numerical work.

It is worth noting that the collisionless Vlasov equation is one in which the 'streaming operator' is hyperbolic and plays the role of advection in *phase space*. When binary collisions are included in the Vlasov equation, one obtains the Boltzmann/Fokker–Planck equation of plasma physics. The Fokker–Planck–Landau Coulomb collision operator is advective–diffusive in character (although in general non-linear). It is plain that at least in the linear limits, the purely collisionless spectral properties of the Vlasov description can be significantly modified by the inclusion of the Landau operator, even at 'low collisionality'. The effective relaxation rates could conceivably be higher than expected from simple collisional (i.e. diffusive in velocity space) decay, by being strongly enhanced by highly sheared advective effects from the streaming terms. These 'velocity space' advection–diffusion effects have not yet been fully explored. Closely related is the notion of 'continuum' damping by shear Alfvén waves, a concept intimately related to the radiation damping of a charged particle in classical electromagnetic theory. These are best illustrated by invoking a small but finite dissipation in the system which 'resolves' the continuum, but nevertheless, the dissipation rate itself becomes independent of the appropriate analogue of the Reynolds number.

Since the advection–diffusion equation itself is a very generic transport equation appearing naturally in transport problems in many different fields, our methods and results can be expected to have a much wider domain of applicability than the original motivation provided by the shear flow paradigm in current tokamak research. Finally, by separating the problem of the genesis of sheared advective flows from that of studying their consequences in a simple but widely applicable setting, valuable insights into the nature of transport and the effects of sheared flows have been attained.

Acknowledgements

The authors would like to thank Terry Martin for his help in the configuration of the Aethelwulf parallel cluster. N.L. acknowledges with thanks, *Fundacao para a Ciencia e a Tecnologia*, *Ministerio da Ciencia e do Ensino Superior*, Portugal for their support. This research was supported by EURATOM and the Department of Trade and Industry, UK.

References

[1] Burrell, K. H., *Science* **281**, 1816 (1998).

[2] Lin, Z. et al., *Phys. Rev. Lett.* **83**, 3645 (1999).

[3] Smolyakov, A. I., Diamond, P. H. and Shevchenko, V. I., *Phys. Plasmas* **7**, 1349 (2000).

[4] Guzdar, P. N., Kleva, R. G. and Chen Liu, *Phys. Plasmas* **8**, 459 (2001).

[5] Thyagaraja, A., *Plasma Phys. Control. Fusion* **42**, B255 (2000).

[6] Lashmore-Davies, C. N., McCarthy, D. R. and Thyagaraja, A., *Phys. Plasmas* **8**, 5121 (2001).

[7] Thyagaraja, A., *J. Plasma Phys.* **59**, 367 (1998).

[8] Parker, E. N. and Thyagaraja, A., *Solar Phys.* **189**, 45 (1999).

[9] Van Kampen, N. G. and Felderhof, B. U., *Theoretical Methods in Plasma Physics*. Amsterdam: North-Holland, 1967.

[10] Titchmarsh, E. C., *Eigenfunction Expansions*, Vol. I. Oxford University Press, 1969.

[11] Abramowitz, M. and Stegun, I. A., *Handbook of Mathematical Functions*. New York: Dover, 1972.

[12] Lortz, D. and Spies, G. O., *Phys. Lett.* **101A**, 7 (1984).

[13] Dewar, R. L. and Davies, B., *J. Plasma Phys.* **32**, 3 (1984).

[14] Kato, T., *Perturbation Theory for Linear Operators*. Berlin: Springer-Verlag, 1976.

[15] Thyagaraja, A. and Haas, F. A., *Physica Scripta* **41**, 693 (1990).

[16] Mantica, P. et al., *Phys. Rev. Lett.* **85**, 4534 (2000).

[17] Townsend, A. A., *The Structure of Turbulent Shear Flow*. Cambridge University Press, 1956.

[18] Lin, C. C., *The Theory of Hydrodynamic Stability*. Cambridge University Press, 1967.

[19] Drazin, P. and Reid, W., *Hydrodynamic Stability*. Cambridge University Press, 1981.